J|A|C|S ARTICLES

Published on Web 11/16/2010

Mass Spectrometry of Ligand Exchange Chelation of the Nanoparticle $[Au_{25}(SCH_2CH_2C_6H_5)_{18}]^{1-}$ by $CH_3C_6H_3(SH)_2$

Christina A. Fields-Zinna,† Joseph F. Parker, and Royce W. Murray*

Kenan Laboratories of Chemistry, University of North Carolina, Chapel Hill, North Carolina 27599, United States

Received July 14, 2010; E-mail: rwm@unc.edu

Abstract: Mass spectrally detected products of ligand exchange reactions of the nanoparticle $[Au_{25}(SC_2H_4C_6H_5)_{18}]^{1-}$, (abbrev. $Au_{25}(SC_2Ph)_{18}$), where the dithiol is toluene-3,4-dithiol, $CH_3C_6H_3(SH)_2$, include nanoparticles containing both doubly (bidentate, or chelating) and singly bonded dithiol. The bidentate binding displaces two of the original $-SC_2Ph$ ligands, and singly bonded dithiol displaces one $-SC_2Ph$ ligand, while maintaining, for mass spectrally detected species, occupancy of 18 ligation sites. Extended exchange reaction times result in an apparent maximum of six chelated dithiolates. In the $Au_{25}(SC_2Ph)_{18}$ nanoparticle, six semi-rings of $-S(R)-Au-S(R)-Au-S(R)-$ act as the protecting ligand shell surrounding a Au_{13} core; the chelation is suggested to involve binding of dithiolates to adjacent semi-rings, rather than to a single semi-ring. Both high resolution ESI and lower resolution MALDI spectra support the product assignments. A minor extent of bidentate ligand incorporation is sufficient to severely compromise the well-known $Au_{25}(SC_2Ph)_{18}$ UV−vis fine structure and to alter its voltammetric pattern, reflecting either associated semi-ring distortion and/or decay of the exchange product.

Introduction

Research on gold nanoparticles is a popular and continuously evolving field due to the interesting optical and electronic properties of these nanoparticles and their possibilities for compositional manipulation of their protecting ligand shells. Applications have been proposed in chemical sensing,[1−5] optoelectronic devices,[6,7] and nanomedicine.[8−11] Gold thiolate-protected nanoparticles are of particular interest given their biocompatibility, chemical stability, and ease of functionalization.

Development of nanoparticles for *in vivo* applications is ongoing; the requirements are challenging, including stability in complex biological media, absence of aggregation, and minimal nonspecific binding. Nanoparticles protected by monothiolate ligands may be more subject to unfavorable chemical changes, including aggregation; the stability issue for the nanoparticles and the labels that they bear may be improved by use of pegylated dithiols.[14] Dithiols are known to bind to planar Au surfaces.[12,13] In such presumed bidentate bindings, the ligands act as chelating agents and should exhibit enhanced equilibrium binding constants for the same entropic reasons as do metal complexes.[15] Thioctic acid can, however, be desorbed from gold nanoparticle surfaces.[16] The above involve assumptions of bidentate binding, but X-ray absorption near edge spectroscopy (XANES) has more explicitly demonstrated the actual binding of both sulfur groups of reduced thioctic acid on gold nanoparticles used as biological probes.[17] Coordination with trithiols has also been explored.[18,19]

Another area in which polythiols pose an impact is in investigation of properties of sulfur−gold bonding in the ligand shells of thiolated Au nanoparticles. Various experiments have probed the structural interaction between sulfur and gold in monothiolate−gold surface structures[20] as well as dithiol−gold

† Current address: Toxicology Section of the Division of Forensic Sciences, Georgia Bureau of Investigation, Decatur, GA 30034.

(1) Lu, Y.; Shi, W.; Qin, J.; Lin, B. *Electrophoresis* **2009**, *30*, 579–582.
(2) Rahman, M. A.; Son, J. I.; Won, M.-S.; Shim, Y.-B. *Anal. Chem.* **2009**, *81*, 6604–6611.
(3) Jena, B. K.; Raj, C. R. *Biosens. Bioelectron.* **2008**, *23*, 1285–1290.
(4) Chai, R.; Yuan, R.; Chai, Y.; Ou, C.; Cao, S.; Li, X. *Talanta* **2008**, *74*, 1330–1336.
(5) Zhao, W.; Chiuman, W.; Lam, J. C. F.; Brook, M. A.; Li, Y. *Chem. Commun.* **2007**, 3729–3731.
(6) Chen, F.-C.; Wu, J.-L.; Lee, C.-L.; Hong, Y.; Kuo, C.-H.; Huang, M. H. *Appl. Phys. Lett.* **2009**, *95*, 013305.
(7) El-Sayed, M. *Acc. Chem. Res.* **2004**, *37*, 326–333.
(8) Prabaharan, M.; Grailer, J. J.; Pilla, S.; Steeber, D. A.; Gong, S. *Biomaterials* **2009**, *30*, 6065–6075.
(9) Agasti, S. S.; Chompoosor, A.; You, C.-C.; Ghosh, P.; Kim, C. K.; Rotello, V. M. *J. Am. Chem. Soc.* **2009**, *131*, 5728–5729.
(10) Park, C.; Youn, H.; Kim, H.; Noh, T.; Kook, Y. H.; Oh, E. T.; Park, H. J.; Kim, C. *J. Mater. Chem* **2009**, *19*, 2310–2315.
(11) Han, G.; Ghosh, P.; De, M.; Rotello, V. *NanoBiotechnology* **2007**, *3*, 40–45.
(12) Garg, N.; Lee, T. R. *Langmuir* **1998**, *14*, 3815–3819.
(13) Nuzzo, R. G.; Allara, D. L. *J. Am. Chem. Soc.* **1983**, *105*, 4481–4483.
(14) Eck, W.; Craig, G.; Sigdel, A.; Ritter, G.; Old, L. J.; Tang, L.; Brennan, M. F.; Allen, P. J.; Mason, M. D. *ACS Nano* **2008**, *2*, 2263–2272.
(15) Busch, D. H. *Chem. Rev.* **1993**, *93*, 847–860.
(16) Lin, S.-Y. L.; Tsai, Y.-T.; Chen, C.-C.; Lin, C.-M.; Chen, C.-h. *J. Phys. Chem. B* **2004**, *108*, 2134–2139.
(17) Roux, S.; Garcia, B.; Bridot, J.-L.; Salome, M.; Marquette, C.; Lemelle, L.; Gillet, P.; Blum, L.; Perriat, P.; Tillement, O. *Langmuir* **2005**, *21*, 2526–2536.
(18) Phares, N.; White, R. J.; Plaxo, K. W. *Anal. Chem.* **2009**, *81*, 1095–1100.
(19) Li, Z.; Jin, R.; Mirkin, C. A.; Letsinger, R. L. *Nucleic Acids Res.* **2002**, *30*, 1558–1562.
(20) Bubnis, G. J.; Cleary, S. M.; Mayne, H. R. *Chem. Phys. Lett.* **2009**, *470*, 289–294.

surface structures.[21] For very small Au nanoparticles, the sulfur−gold interface is now known to be more complex than the standard analogy to self-assembled alkanethiolate monolayers on planar Au(111) surfaces.[22] On small thiolate-protected Au nanoparticles, the thiolate is coordinated in a bridging configuration, in $Au_{CORE}-S(R)-Au-S(R)-Au_{CORE}$ and $Au_{CORE}-S(R)-Au-S(R)-Au-S(R)-Au_{CORE}$ surface structures, which act as the protecting ligands of Au_{102} and Au_{25} nanoparticles, respectively (also termed "staples" and "semi-rings").[23,24] These surface structures have been demonstrated by crystallographic determinations and are also predicted theoretically.[26,27] The behavior and properties of these important surface structures, which may well extend[28] to larger Au−thiolate nanostructures, are an evolving picture that invites further probing. Because the nanoparticle $[Au_{25}(SC_2H_4C_6H_5)_{18}]^{1-}$ (abbrev. $Au_{25}(SC_2Ph)_{18}$) is readily accessible, with a formula well established by mass spectra[25] and a crystallographically demonstrated structure,[24] it is a useful model with which to explore the formation of bidentate-bound thiolate nanoparticle ligands, which has not previously been definitively accomplished.

This Article specifically demonstrates, by mass spectral observations, that the ligand exchange reaction incorporation of toluene-3,4-dithiol ($CH_3C_6H_3(SH)_2$) occurs as both a bidentate or chelating ligand (e.g., $CH_3C_6H_3(S-)_2$) and a monodentate ligand (e.g., $CH_3C_6H_3(SH)(S-)$) onto $[Au_{25}(SC_2H_4C_6H_5)_{18}]^{1-}$ (abbrev. $Au_{25}(SC_2Ph)_{18}$ or $Au_{25}L_{18}$). The former circumstance displaces two of the original $-SC_2Ph$ ligands, and in the latter, one original ligand, maintaining an overall occupancy of 18 ligation sites, as seen for spectrally detected species. The initial average nanoparticle mass is 7394 Da; one bidentate $CH_3C_6H_3(S-)_2$ binding produces a mass loss of 120 Da, and one monodentate $CH_3C_6H_3(SH)(S-)$ binding causes a mass gain of 18 Da. The balance between the two kinds of exchange depends on the specific reaction conditions. Extended exchange reactions result in an apparent maximum of six chelating dithiolates, implying an average of one per $Au_{CORE}-S(R)-Au-S(R)-Au-S(R)-Au_{CORE}$ semi-ring. We suggest that the bite angle of the $CH_3C_6H_3(S-)_2$ ligand is more conducive to binding of this dithiolate to adjacent $-S(R)-Au-S(R)-Au-S(R)-$ semi-rings, as opposed to dithiolate binding to a single semi-ring. Both high resolution ESI and lower resolution MALDI spectra are obtained to support the product assignments.

Changes in nanoparticle UV−vis spectra and voltammetry during the ligand exchange processes lead to the conclusion that only a minor extent of bidentate exchange is sufficient to severely compromise the well-known $Au_{25}(SC_2Ph)_{18}$ UV−vis fine structure and to severely alter its voltammetric pattern. The semi-rings may experience some distortion upon binding to this particular dithiolate ligand, and/or some forms of the exchange product are unstable.

Experimental Section

Chemicals. Phenylethanethiol ($HSCH_2CH_2Ph$, or HSC_2Ph, 98%), toluene-3,4-dithiol ($CH_3C_6H_3(SH)_2$, 90%), thiophenol (HSC_6H_5, 97%), tetrabutylammonium perchlorate (Bu_4NClO_4, >99%), tetra-*n*-octylammonium bromide (Oct_4NBr, 98%), sodium borohydride ($NaBH_4$, 99%), cesium acetate (CsOAc, 99.9%), and *trans*-2-[3-(4-*tert*-butylphenyl)-2-methyl-2-propenylidene] malononitrile (DCTB, MALDI matrix) were obtained from Sigma-Aldrich. Certified ACS toluene, optima methylene chloride, optima methanol, optima acetonitrile, and absolute ethanol (Fischer) were used as received. Water was purified with a Barnstead NANOpure system (18 MΩ). Hydrogen tetrachloroaurate trihydrate (from 99.999% pure gold) was prepared by a literature procedure[29] and stored in a freezer at −20 °C.

Synthesis of Nanoparticles $[Oct_4N]^+[Au_{25}(SCH_2CH_2Ph)_{18}]^-$. $[Oct_4N]^+[Au_{25}(SCH_2CH_2Ph)_{18}]^-$ (abbrev. $Au_{25}(SC_2Ph)_{18}$) nanoparticles were synthesized as previously reported, for most experiments.[30] (In the cited paper, the nanoparticle was wrongly assigned as being $Au_{38}(SCH_2CH_2Ph)_{24}$; the corrected assignment was made from mass spectral observations[25,32]). For example, $AuCl_4^-$ (as 1.9 g of HAuCl4) was transferred from an aqueous phase to 45 mM Oct_4NBr in toluene (126 mL), and after adding 2.17 mL of phenylethanethiol (HSC2Ph, mass = 137 Da; thiol:Au mole ratio 3.2:1), it was stirred in toluene overnight. The colorless solution, cooled to 0 °C in an ice water bath, was mixed quickly with 2.4 g of $NaBH_4$ in 38 mL of ice cold Nanopure water, and the mixture was stirred vigorously for 24 h. Discarding the aqueous layer, the organic layer was washed three times with Nanopure water, and rotovapped to a viscous sludge, which was extracted with ethanol (2 h) to remove excess ligand and larger nanoparticles. The ethanol-insoluble portion, containing the small-sized nanoparticles, was purified using repeated solvent fractionation, dissolving the small nanoparticles in acetonitrile and reprecipitating by methanol addition. A newer synthetic procedure[33a] was used to prepare the $Au_{25}(SC_2Ph)_{18}$ nanoparticles used in Figures S-2 and S-3. $HAuCl_4 \cdot 3H_2O$ (1.00 g, 2.54 mmol) and *tetra-n*-octylammonium bromide (Oct_4NBr, 1.56 g, 2.85 mmol) were codissolved in tetrahydrofuran (THF, 70 mL), stirred for 15 min, and then phenylethanethiol (1.80 mL, 13.4 mmol) was added (room temperature) and the mixture was stirred for at least 12 h (colorless solution). Sodium borohydride ($NaBH_4$, 0.967 g, 25.6 mmol) in 24 mL of Nanopure water was stirred at 0 °C for 1 h, then rapidly added to the THF solution, and quietly stirred for at least 48 h. The solution color evolves from blackish to a murky brown, which is indicative of a high proportion of the $Au_{25}(S(CH_2)_2Ph)_{18}^-$ anion. The product solution was gravity filtered and then rotovapped to remove the THF. The product was taken up into 30 mL of toluene and washed five times with 150 mL of Nanopure water in a separatory funnel, rotovapped to remove the toluene, and the solid was washed thoroughly with methanol to remove any traces of excess thiol and Oct_4NBr. The product is pure $[Oct_4N]^+[Au_{25}(S(CH_2)_2Ph)_{18}]^-$ (243 mg, 30% yield by Au).

(21) Yokokawa, S.; Tamada, K.; Ito, E.; Hara, M. *J. Phys. Chem. B* **2003**, *107*, 3544–3551.
(22) Ulman, A. *Chem. Rev.* **1996**, *96*, 1533–1554.
(23) Jadzinsky, P. D.; Calero, G.; Ackerson, C. J.; Bushnell, D. A.; Kornberg, R. D. *Science* **2007**, *318*, 430–433.
(24) Heaven, M. W.; Dass, A.; White, P. S.; Holt, K. M.; Murray, R. W. *J. Am. Chem. Soc.* **2008**, *130*, 3754–3755.
(25) Fields-Zinna, C. A.; Sampson, J. S.; Crowe, M. C.; Tracy, J. B.; Parker, J. F.; deNey, A. M.; Muddiman, D. C.; Murray, R. W. *J. Am. Chem. Soc.* **2009**, *131*, 13844–13851.
(26) Akola, J.; Walter, M.; Whetten, R. L.; Häkkinen, H.; Grönbeck, H. *J. Am. Chem. Soc.* **2008**, *130*, 3756–3757.
(27) Walter, M.; Akola, J.; Lopez-Acevedo, O.; Jadzinsky, P. D.; Calero, G.; Ackerson, C. J.; Whetten, R. L.; Grönbeck, H.; Häkkinen, H. *Proc. Natl. Acad. Sci. U.S.A.* **2008**, *105*, 9157–9162.
(28) (a) Lopez-Acevedo, O.; Akola, J.; Whetten, R. L.; Grönbeck, H.; Häkkinen, H. *J. Phys. Chem. C* **2009**, *113*, 5035–5038. (b) Grönbeck, H.; Häkkinen, H.; Whetten, R. L. *J. Phys. Chem. C* **2008**, *112*, 15940–15942.
(29) Brauer, G. *Handbook of Preparative Inorganic Chemistry*; Academic Press: New York, 1965.
(30) Donkers, R. L.; Lee, D.; Murray, R. W. *Langmuir* **2004**, *20*, 1945–1952.
(31) Hostetler, M. J.; Templeton, A. C.; Murray, R. W. *Langmuir* **1999**, *15*, 3782–3789.
(32) Tracy, J. B.; Crowe, M. C.; Parker, J. F.; Hampe, O.; Fields-Zinna, C. A.; Dass, A.; Murray, R. W. *J. Am. Chem. Soc.* **2007**, *129*, 16209–16215.
(33) (a) Parker, J. F.; Weaver, J. E. F.; McCallum, F.; Fields-Zinna, C. F.; Murray, R. W. *Langmuir* **2010**, *26*, 13650−13654. (b) Wu, Z.; Suhan, J.; Jin, R. *J. Mater. Chem.* **2009**, *19*, 622–626.

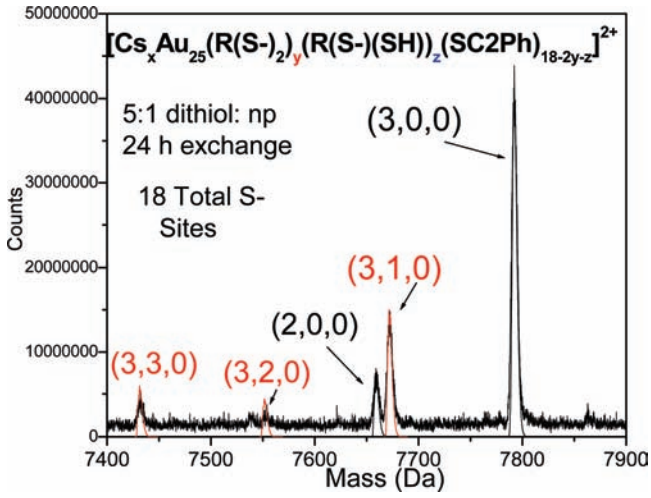

Figure 1. ESI-QQQ mass spectrum of $Au_{25}(SC2Ph)_{18}$ exchanged with toluene-3,4-dithiol ($CH_3C_6H_3(SH)_2$) at a 5:1 mol ratio of dithiol:nanoparticle for 24 h. Specifically, 7 μL (or 0.67 μmol) of dithiol was added to about 1 mg (or 0.14 μmol) of $Au_{25}(SC2Ph)_{18}$ sample dissolved in ca. 200 μL of methylene chloride and stirred for 24 h. The dithiol is capable of either bidentate binding ($CH_3C_6H_3(S-)_2$, or $R(S-)_2$) or monodentate binding ($CH_3C_6H_3(S-)(SH)$ or $R(S-)(SH)$). ESI cationization was achieved by addition of cesium acetate, which might limit the types of products detected. In this figure, *y* is the number of bidentate dithiolates ($R(S-)_2$), and *z* is the number of monodentate dithiolates ($R(S-)(SH)$). The number of Cs^+ ions attributing charge to the nanoparticle is indicated by *x*, and the number of remaining (SC2Ph) ligands is $18 - 2y - z$. Labels in red indicate occurrence of bidentate bonding.

Ligand Exchange Reactions. The dithiol toluene-3,4-dithiol, $CH_3C_6H_3(SH)_2$ (mass = 156.27 Da), was reacted with $Au_{25}(SC_2Ph)_{18}$ under several ligand exchange[31,32] reaction conditions.

For mass spectra in Figure 1, 7 μL (0.67 μmol) of the dithiol and 1 mg (0.14 μmol) of $Au_{25}(SC_2Ph)_{18}$ codissolved in 200 μL of CH_2Cl_2 (5:1 dithiol:nanoparticle mole ratio; 0.3:1 dithiol:SC_2Ph mole ratio; nanoparticle concentration 0.7 mM) were stirred for 24 h. For Figure 2 data, the Figure 1 procedure was performed twice, with an intervening cleaning of the product with a heptane wash.

For the mass spectra in Figures 3, 4, and 6 and Table 1, 12.7 μL (1.21 μmol) of the dithiol codissolved with 1 mg (0.14 μmol) of $Au_{25}(SC_2Ph)_{18}$ in 200 μL of CH_2Cl_2 (9:1 dithiol:nanoparticle mole ratio; ~0.5:1 dithiol:SC_2Ph mole ratio; nanoparticle concentration 0.7 mM) was stirred for either 30 min or 4 h, and then dried on a rotary evaporator. Excess ligand was removed by washing several times with heptane.

The mass spectra in Figure S-2, and the electrochemical and optical data in Figures 7 and S-4 (experiments done separately), were obtained using much lower exchange concentrations than those preceding and involve longer time increments of exchange. 0.48 μL (3.6 μmol) of dithiol was added to ~2 mL of 0.2 mM $Au_{25}(SC_2Ph)_{18}$ nanoparticles in CH_2Cl_2 and stirred for the times indicated in the Figures 7, S-2, and S-4 in separate experiments. Samples were taken from the reaction solutions for the mass spectral and optical experiments. 0.1 M Bu_4NClO_4 electrolyte was present in the experiments of Figures 7 and S-4, but not in the mass spectrometry experiment of Figure S-2.

Ligand exchange of $Au_{25}(SC_2Ph)_{18}$ with thiophenol was at a mole ratio of 18:1 thiophenol:nanoparticle and an exchange time of ca. 24 h, CH_2Cl_2.

Voltammetry and Optical Spectra. Osteryoung square-wave voltammetry (OSWV)[34] was performed with a Bioanalytical Systems instrument (BAS-100B) on 0.2 mM nanoparticle/0.1 M Bu_4NClO_4/CH_2Cl_2 solutions, under Ar, with 0.15 cm diameter Pt disk working, Pt wire counter, and Ag/AgCl (aq) reference electrodes. The working electrode was polished (0.05 μm alumina or 1/4 μm diamond paste) and cleaned electrochemically by cycling in 0.1 M H_2SO_4 between potential limits of 1200 and −610 mV.[34]

UV−vis spectra were taken with a Shimadzu UV−vis model UV-1601 spectrophotometer. Data for Figure S-4 were taken in conjunction with the voltammetry of Figure 7, diluting aliquots (ca.

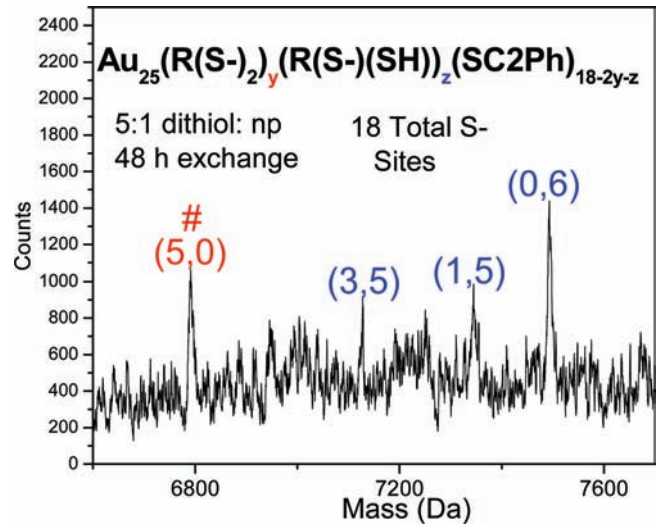

Figure 2. MALDI spectrum of 5:1 dithiol:nanoparticle for 48 h exchange. Specifically, 7 μL (or 0.67 μmol) of dithiol was added to ca. 1 mg (or 0.14 μmol) of $Au_{25}(SC2Ph)_{18}$ sample dissolved in about 200 μL of methylene chloride and stirred for 24 h. The sample was then cleaned with heptane, and the above procedure was performed again. In this figure, *y* is the number of bidentate dithiols, and *z* is the number of monodentate dithiols. The number of remaining (SC2Ph) ligands is $18 - 2y - z$. Labels in red indicate predominantly bidentate bonding, and blue labels indicate predominantly monodentate bonding. The absence of the initial $Au_{25}(SC2Ph)_{18}$ nanoparticle peak at 7394 Da suggests its exhaustive consumption.

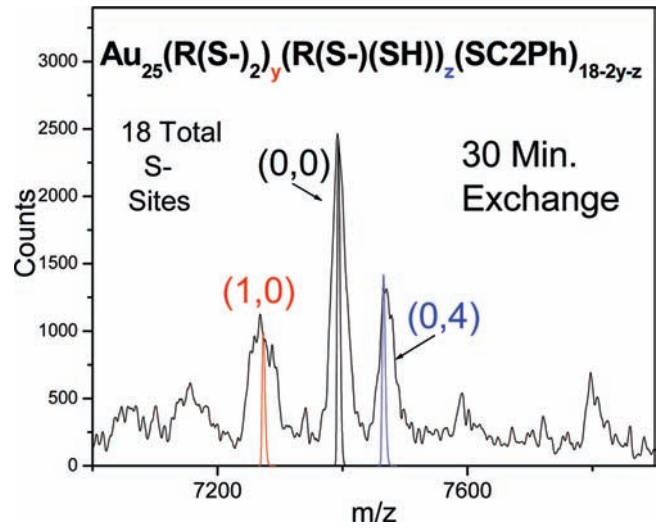

Figure 3. MALDI mass spectrum of $Au_{25}(SC2Ph)_{18}$ after a 30 min exchange with $CH_3C_6H_3(SH)_2$, at 0.7 mM nanoparticle concentration. Specifically, 12.7 μL (or 1.21 μmol) of the dithiol was added to about 1 mg (or 0.14 μmol) of $Au_{25}(SC2Ph)_{18}$ nanoparticle dissolved in ca. 200 μL of methylene chloride. After 30 min exchange, the solution was dried and washed several times with heptane. Species detected include unexchanged nanoparticle, as well as chelated and nonchelated exchange products (see Table 1). Simulations (in red, black, and blue) support the assignments shown. Red (simulations and labels) indicates bidentate binding, black indicates no dithiol exchange, and blue indicates monodentate binding.

(34) Bard, A. J.; Faulkner, L. R. *Electrochemical Methods: Fundamentals and Applications*, 2nd ed.; John Wiley and Sons: New York, 1980.

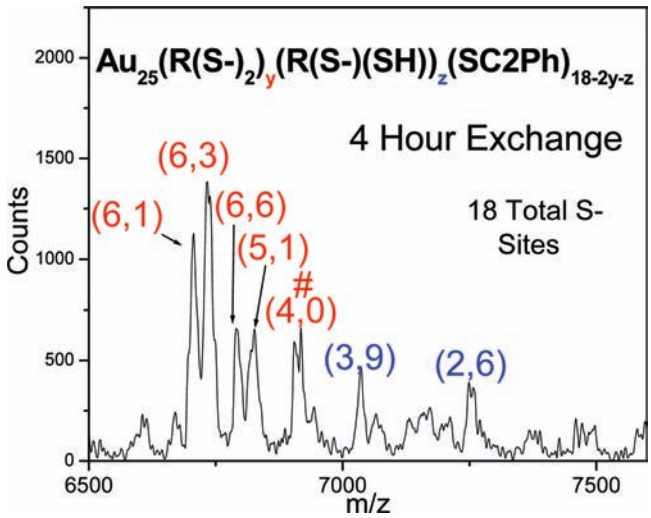

Figure 4. MALDI mass spectrum of $Au_{25}(SC2Ph)_{18}$ after a 4 h exchange with $CH_3C_6H_3(SH)_2$ at 0.7 mM nanoparticle concentration. Specifically, 12.7 μL (or 1.21 μmol) of the dithiol was added to ca. 1 mg (or 0.14 μmol) of $Au_{25}(SC2Ph)_{18}$ nanoparticle dissolved in ca. 200 μL of methylene chloride. After 4 h exchange, the solution was dried and washed several times with heptane. Notation dictates that *y* is the number of bidentate dithiols and *z* is the number of monodentate dithiols. Red labels indicate exchange products with mostly bidentate binding, and blues labels indicate primarily monodentate binding. "#" indicates solely bidentate binding. The peak assignments indicate mixtures of bidentate and monodentate binding; see Table 1.

Table 1. List of Species in MALDI Mass Spectra (Figures 3 and 4) for 30 min and 4 h Ligand Exchanges of $Au_{25}(SC2Ph)_{18}$ with $CH_3C_6H_3(SH)_2$, a Dithiol Capable of Either Bidentate Bonding ($CH_3C_6H_3(S-)_2$) or Monodentate Bonding ($CH_3C_6H_3(S-)(SH)$)[a]

	total ligand (S−) sites: 18 (bidentate ligand coordinates 2 sites)				
Au_{25} species	number bidentate $(S-)_2$	number monodentate (S−)(SH)	number −SC2Ph	observed masses (Da)	simulated masses (Da)
		30 min Exchange			
(0,4)	0	4	14	7466	7465
(1,0)	1	0	16	7269	7273
		4 h Exchange			
(2,6)	2	6	8	7255	7254
(3,9)	4	7	3	7036	7038
(4,0)	4	0	10	6910	6912
(5,1)	5	1	7	6818	6810
(6,6)	6	6	0	6787	6780
(6,3)	6	3	3	6730	6726
(6,1)	6	1	5	6704	6690

[a] 12.7 μL (or 1.21 μmol) of the dithiol was added to about 1 mg (or 0.14 μmol; 0.7 mM) of $Au_{25}(SC2Ph)_{18}$ sample dissolved in ca. 200 μL of methylene chloride (a 9:1 dithiol:nanoparticle mole ratio, or 0.5:1 dithiol:SC2Ph mole ratio). This was stirred for 30 min and 4 h, dried on a rotary evaporator, and excess ligand was removed by washing several times with heptane. It is assumed that the total number of coordination sites remains 18. Observed and simulated masses are presented; observed masses are affected by error in mass accuracy and low resolution of instrument.

60 μL) from the electrochemical cell in *ca.* 3 mL of CH_2Cl_2 and taking the spectra immediately.

Mass Spectrometry. Matrix-assisted laser desorption/ionization (MALDI) mass spectra were collected on a Voyager DE Biospectrometry Workstation (Perspective Biosystems, Inc., Framingham, MA) in the linear mode using a nitrogen laser (337 nm) and *trans*-2-[3-(4-*tert*-butylphenyl)-2-methyl-2-propenylidene] malononitrile (DCTB)[35] as the matrix. Spectra were obtained in negative ion mode using an acceleration voltage of 25 kV and delay time of 350 ns, and at serially reduced laser pulse intensities (laser fluence) to minimize nanoparticle fragmentation, as done before.[35] The data were smoothed by Savitsky-Golay 17-point quadratic method.[36] Simulated high resolution mass spectra were produced using a publicly available Molecular Weight Calculator.[37]

Positive-mode electrospray spectra (ESI-QQQ-MS) were obtained on a Micromass Quattro II, a triple quad mass spectrometer with a nanoelectrospray ionization source. Cesium acetate was added as a charging agent at 80:1 salt:nanoparticle mole ratio into a 50 μM dithiol-exchanged $Au_{25}(SC_2Ph)_{18}$ 70:30 methanol:toluene solution. Data were processed as above.

Results and Discussion

The mass spectra results presented describe exchange reactions of the dithiol $CH_3C_6H_3(SH)_2$ with the $Au_{25}(SC_2Ph)_{18}$ ligand shell, where the reactions were conducted to different extents of exchange by varying reaction time and feed ratios of ligand to nanoparticle. The objective was to determine the occurrence, and relative incidence, of bidentate binding ($CH_3C_6H_3(S-)_2$) and monodentate binding (($CH_3C_6H_3(S-)(SH)$), and additionally to see how incorporation of this ligand affects the UV−vis and voltammetric nanoparticle properties.

Two initial experiments were conducted over long reaction times (24 and 48 h, Figures 1 and 2), at (low) 5:1 mol ratio of dithiol to nanoparticle. The 24 h exchange experiment of Figure 1 was observed using a high resolution ESI-QQQ spectrometer. The second experiment was another 24 h exchange reaction of products isolated from the Figure 1 reaction (e.g., total 48 h exchange) and was observed (Figure 2) using a lower resolution MALDI approach.

The results of Figure 1 firmly establish that bidentate (chelating) binding of the dithiol occurs. The assignment coding is x = no. of Cs^+ ions, y = number of bidentate ligands $CH_3C_6H_3(S-)_2$, and z = number of monodentate ligands $CH_3C_6H_3(S-)(SH)$. The number of remaining $-SC_2Ph$ ligands is $18 - 2y - z$. The Figure 1 (3,0,0) and (2,0,0) peaks are unreacted $Au_{25}(SC_2Ph)_{18}$ (anion and neutral state) charged by association to three and two, respectively, Cs^+ ions. Assignment of these peaks has been unambiguously established in earlier experiments.[25] Figure 1 also shows three peaks, red labels (3,1,0), (3,2,0), and (3,3,0), each shifted to 120 Da lower mass by successive bidentate binding of $CH_3C_6H_3(S-)_2$. The low resolution simulations of the (3,1,0), (3,2,0), and (3,3,0) peaks are shown in red in Figure 1, and a high resolution simulation is compared to the (3,1,0) peak in Figure S-1 (red curve, see the Supporting Information) on a scale showing its close-to-isotopic resolution.

No peaks could be identified in Figure 1 that corresponded to monodentate binding of $CH_3C_6H_3(S-)(SH)$. Binding of a single $CH_3C_6H_3(S-)(SH)$ ligand with loss of a $-SC_2Ph$ ligand would produce a peak at 7810.9 Da (18 Da heavier), which is not seen. (Binding of a single $CH_3C_6H_3(S-)(SH)$ ligand with loss of two $-SC_2Ph$ ligands (e.g., 3,0,1) would produce a peak at 7673.7 Da, including 3 Cs^+ ions, close to (but not matching as well) the high resolution (3,1,0) peak shown in Figure S-1, but would also correspond to a nanoparticle with a total of 17 ligation sites, which we feel unlikely.)

The key results of Figure 1 are then that (a) a bidentate binding is demonstrated on the $Au_{25}L_{18}$ nanoparticle, and (b) at

(35) Dass, A.; Stevenson, A.; Dubay, G. R.; Tracy, J. B.; Murray, R. W. *J. Am. Chem. Soc.* **2008**, *130*, 5940–5946.
(36) Savitzky, A. G., M. J. E. *Anal. Chem.* **1964**, *36*, 1627.
(37) Monroe, M. Biological Mass Spectra Data and Software Distribution Center Website. http://omics.pnl.gov/software/MWCalculator.php.

early stages of exchange at least it is the preferred form (rather than monodentate). This preference is not unlike that seen in metal complex coordination chemistry involving bidentate-capable ligands.

The Figure 1 exchange reaction is extended to 48 h in Figure 2 where, as in all subsequent experiments presented, detection of the nanoparticle products is accomplished using MALDI. This assumes that isolation of the 24 h exchange product occurs without loss of any material, so the experiment differs from one where the reaction time was an uninterrupted 48 h. Also, the differing modes of charging in Figures 1 and 2 may mean that some exchange products seen in Figure 2 may not have been fully detected in Figure 1. The Figure 2 spectrum, although nonoptimized and rather noisy, nonetheless shows several informative peaks. MALDI spectra of $Au_{25}(SC2Ph)_{18}$ nanoparticles with the DCTB matrix have previously produced[35] solely 1+ ions, which was assumed in the assignments. The (*y*,*z*) peak notation is like that in Figure 1, denoting the numbers of bidentate and monodentate ligands resulting in the exchange. A (0,0) peak for the parent nanoparticle (7394 Da) is absent; it has apparently been consumed by exchanges. Now, monodentate as well as bidentate exchange products can be seen, in the (5,0), (3,5), and (1,5) peaks. Interestingly, a substantial peak of solely monodentate-exchanged nanoparticles (0,6) is observed, and the (3,5) and (1,5) show the occurrence of combined bidentate and monodentate exchange products.

A further analysis of the $Au_{25}(SC_2Ph)_{18}$ exchange reaction with the $CH_3C_6H_3(SH)_2$ dithiol was afforded by MALDI observations at shorter reaction times (30 min and 4 h) and at a larger (9:1) dithiol:nanoparticle mole ratio (meaning a faster exchange rate). Figures 3 and 4 show the MALDI mass spectra of the two exchange products. From the 30 min exchange product, a prominent peak is seen for the parent nanoparticle $Au_{25}(SC2Ph)_{18}$, with a peak also seen at 120 Da lower mass for a bidentate ($CH_3C_6H_3(S-)_2$) bound product (1,0). Another assignment is made for a solely monodentate-bound exchange product (0,4). However, in the latter assignment, considering the mass increase (18 Da) expected for each monodentate exchange of $CH_3C_6H_3(S-)(SH)$ ligand for $-SC_2Ph$, the (0,4) peak width is sufficiently broad that it may also include some (0,5) exchange products. MALDI detection of the numbers of monodentate exchange products is less exacting than that of bidentate exchanges due to the smaller mass change (18 vs 120 Da).

Continuing the exchange reaction to 4 h produced the spectrum of Figure 4, which shows that the extents of both bidentate and monodentate binding increase, and that nanoparticles with mixed bidentate and monodentate exchange product shells have been formed (as in Figure 2).

Table 1 lists the species observed in Figures 3 and 4 based on the number of bidentate ligands, monodentate ligands, and (SC_2Ph) ligands. Clearly associated with the higher numbers of bidentate ligands are higher numbers also of monodentate ligands, but with a maximum of 18 binding sites. The extent to which monodentate binding mixes in with concurrent bidentate binding is probably influenced by the fact that multiple ligand exchanges involve statistics of available sites.[31,38−40] When two

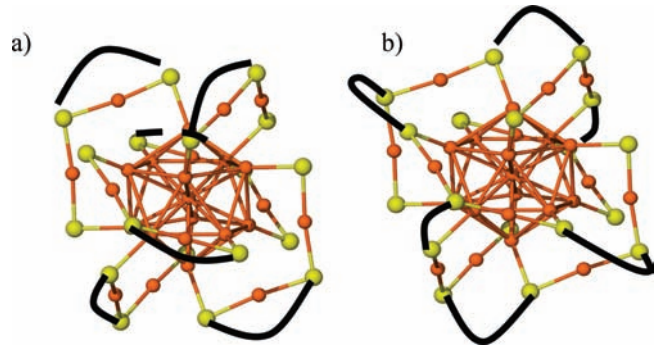

Figure 5. Cartoons of possible configurations of dithiols binding on $Au_{25}L_{18}$. Yellow spheres are sulfur (S) atoms, and orange spheres are gold (Au) atoms. Au_2S_3 represents a semi-ring, and the black, curved lines represent bidentate bound dithiol. (a) This cartoon illustrates bidentate binding within a single semi-ring, and (b) this represents examples of bidentate binding between two different semi-rings, which conceivably involve both the corner and the center Au sites of the semi-rings.

sites with a defined geometrical proximity to one another are consumed per bidentate exchange, the pattern and location of available sites become no longer independent of prior exchanges, especially for small populations of exchangeable sites. It is reasonable then that the location pattern of in-coming both mono- and bidentate coordinations encounters increasingly nonrandom constraints as the extent of ligand exchange continues. Additionally, an initial bidentate or monodentate binding to a given nanoparticle may bias that nanoparticle toward subsequent binding modes. Two important general observations from Table 1 data are that (a) a maximum of six bidentate exchange products are observed (e.g., the (6,1), (6,3), and (6,6) exchange products), and (b) monodentate exchanged products can occupy all of the ligand binding sites remaining from occupancy by six bidentate-bound dithiolate ligands $CH_3C_6H_3(S-)_2$ (the (6,6) exchange result).

The above results, in the context of the known structure of the $Au_{25}(SC_2Ph)_{18}^-$ nanoparticle, with its six $-S(R)-Au-S(R)-Au-S(R)-$ semi-rings,[24] strongly suggest that the protecting shell of six semi-rings remains intact following the bidentate and monodentate ligand exchanges, and reflect the geometrical constraints of an average of one bidentate ligand binding per semi-ring. Within the context of an apparent limit of six bidentate bindings, let us consider how bidentate binding of the dithiolate to the semi-rings might occur. It might involve a dithiolate bound to a single semi-ring, as in the cartoon of Figure 5a, or binding to adjacent semi-rings as in the cartoon of Figure 5b. We have not conducted exact geometrical simulations, which should include consideration of the flexibility (puckering[33a]) of the semi-rings and energetics associated with nonoptimal ligand−S−Au bond angles. Simple modeling suggests that the "bite" angle of the dithiolate, if bound to a single semi-ring, would impose more conformational distortion than would occur if bound to two adjacent semi-rings (Figure 5b). Figure 5b is thus suggested as a more likely binding mode.

Figure S-2a (Supporting Information) shows another exchange experiment tracked by MALDI at high laser fluences, which produce mild nanoparticle fragmentation as seen before.[35] The interesting aspect of this figure is the detection of bidentate exchange products in the fragmented nanoparticles. Figure S-2b in the Supporting Information displays a spectrum obtained in reflectron mode, matched with a simulation that supports the assignment of $Au_{21}(S2)_4(SC2Ph)_{11}$ in Figure S-2a.

(38) Dass, A.; Holt, K.; Parker, J. F.; Feldberg, S. W.; Murray, R. W. *J. Phys. Chem. C* **2008**, *112*, 20276–20283.
(39) Guo, R.; Song, Y.; Wang, G.; Murray, R. W. *J. Am. Chem. Soc.* **2005**, *127*, 2752–2757.
(40) Song, Y.; Huang, T.; Murray, R. W. *J. Am. Chem. Soc.* **2003**, *125*, 11694–11701.

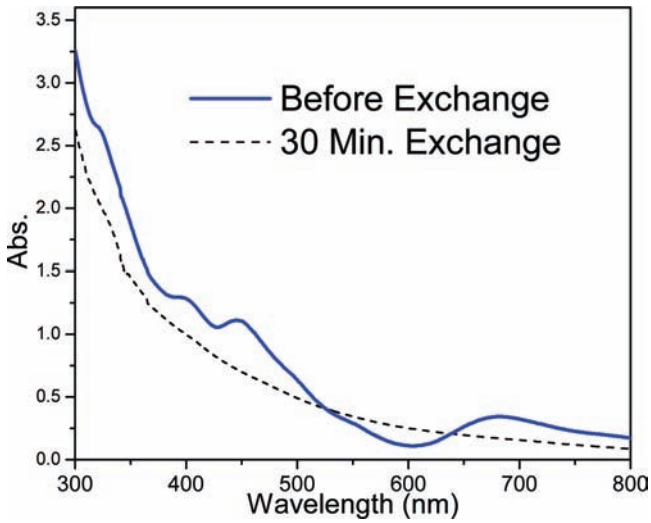

Figure 6. UV−vis spectra of original nanoparticle and of exchange products after 30 min, following cleanup of the nanoparticle product. 12.7 μL (or 1.21 μmol) of the dithiol was added to ca. 1 mg (or 0.14 μmol; 0.7 mM) of $Au_{25}(SC2Ph)_{18}$ nanoparticle dissolved in ca. 200 μL of methylene chloride (a 9:1 dithiol:nanoparticle mole ratio, or 0.5:1 dithiol:SC2Ph mole ratio). The reaction mixture was stirred for 30 min, dried on a rotary evaporator, and excess ligand was removed by washing several times with heptane. These are the same products as those studied in the MALDI data of the Figure 3. After 30 min of exchange, the typical features seen for $Au_{25}(SC2Ph)_{18}$ ("before exchange") have been completely lost (dashed line).

Consider next how ligand exchanges like the above affect the nanoparticle optical and electrochemical properties. Figure 6 shows the UV−vis spectrum of the parent $Au_{25}(SC_2Ph)_{18}^-$ nanoparticle, and the spectrum of the product obtained from the 30 min ligand exchange conducted for the MALDI experiment of Figure 3. Obviously, the fine structure associated with the parent nanoparticle is gone from the electronic spectrum. Monodentate binding does not evoke such an effect; as shown by Figure S-3 (see the Supporting Information), the product from an exchange reaction with thiophenol, which can only exchange via monodentate binding, does not substantially alter the electronic spectral fine structure known for the parent nanoparticle. This suggests that a single bidentate binding can provoke the spectral smoothing result of Figure 6. (Figure S-4 shows the time progression of spectral changes in a different experiment.) Figures 3 and 6 are not self-contradictory; while Figure 3 shows that a substantial amount of parent nanoparticle, and mono- and bidentate exchanged nanoparticles, remains in the isolated exchange product, the overlapping optical spectrum of a bidentate exchange product, or of its decomposition products, could obscure the original spectral fine structure. Decomposition of $Au_{25}(SC_2Ph)_{18}^-$ upon exchange with a different dithiol ligand[41] has been inferred from analogous spectral changes; because we do not know what the bidentate spectra should be, such inference about decomposition here involves an assumption.

(41) Si, S.; Gautier, C.; Boudon, J.; Taras, R.; Gladiali, S.; Burgi, T. *J. Phys. Chem. C* **2009**, *113*, 12966–12969.

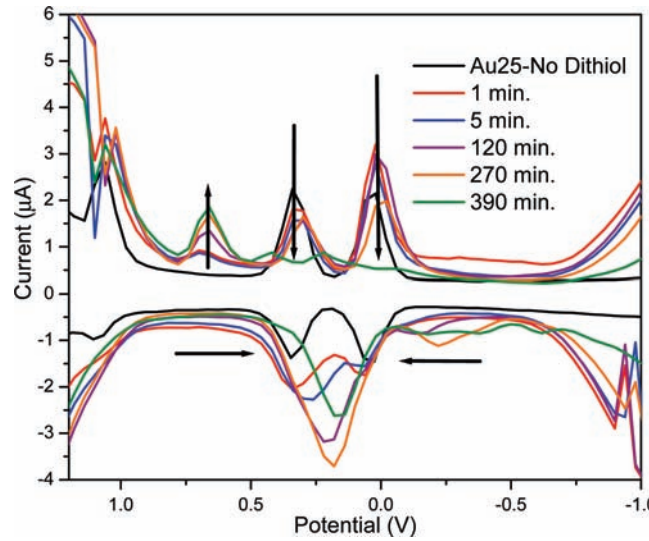

Figure 7. Voltammetry of ligand exchange performed at 0.2 mM nanoparticle in methylene chloride, where a 0.48 μL (3.6 μmol) aliquot of dithiol (which is a liquid) is added to about 2 mL, and measurements are taken at indicated time intervals while stirring. The arrows indicate the general trends of peak amplitude as exchange proceeds.

Voltammetry is presented in Figure 7 for a further exchange reaction done at lowered nanoparticle concentration and 9:1 mole ratio of dithiol:nanoparticle. The reaction thus proceeds quite rapidly, and the voltammetric observations were conducted without isolation or cleanup of the exchange products. Like the optical spectra, severe changes occur, but all features do not vanish. The original doublet of oxidation waves rather quickly decreases in amplitude and is replaced by a single, combined peak at 0.18 V. The associated reduction peaks persist for a longer period of reaction time, but also decrease in amplitude. At the longest observed time, the reduction peaks are gone, and a variety of additional voltammetric features have appeared. It is not possible to interpret these changes without isolating and fractionating products, which was not attempted. The main message is that the electronic structures of the dithiol exchange reaction products have been substantially perturbed, which is consistent with the results of Figure 6.

Finally, while the bidentate dithiolate binding is demonstrated by the mass spectral evidence, it results in severe distortion of both standard electrochemical and optical features for Au_{25}. Bidentate binding must distort the semi-rings that act as the stabilizing features of the nanoparticle. Theoretical data exploring the possibility for distortion would be welcome.

Acknowledgment. This research was supported in part by the National Science Foundation.

Supporting Information Available: Supplementary mass and optical spectra. This material is available free of charge via the Internet at http://pubs.acs.org.

JA106243G